



**HAL**  
open science

# Discovery of necklace-like links made of dislocations - Supporting Informations

Pawel Pieranski, Maria Helena Godinho

► **To cite this version:**

Pawel Pieranski, Maria Helena Godinho. Discovery of necklace-like links made of dislocations - Supporting Informations. 2024. hal-04828550

**HAL Id: hal-04828550**

**<https://hal.science/hal-04828550v1>**

Preprint submitted on 10 Dec 2024

**HAL** is a multi-disciplinary open access archive for the deposit and dissemination of scientific research documents, whether they are published or not. The documents may come from teaching and research institutions in France or abroad, or from public or private research centers.

L'archive ouverte pluridisciplinaire **HAL**, est destinée au dépôt et à la diffusion de documents scientifiques de niveau recherche, publiés ou non, émanant des établissements d'enseignement et de recherche français ou étrangers, des laboratoires publics ou privés.

1

# 2 **Supporting Information for**

## 3 **Discovery of necklace-like links made of dislocations**

4 **P. Pieranski and M.H. Godinho**

5 **Pawel Pieranski.**

6 **E-mail: [pawel.pieranski@universite-paris-saclay.fr](mailto:pawel.pieranski@universite-paris-saclay.fr)**

### 7 **This PDF file includes:**

- 8 Supporting text
- 9 Figs. S1 to S10
- 10 Legends for Movies S1 to S12
- 11 SI References

### 12 **Other supporting materials for this manuscript include the following:**

- 13 Movies S1 to S12

## 14 Supporting Information Text

### 15 1. Topological decay of entanglements of superfluid vortices

16 **A. Theoretical expectations.** The topological decay of knotted and linked superfluid vortices plays the  
17 main role during the decay of the turbulence in superfluids (1, 2). It was explored both experimentally  
18 and theoretically. Kleckner et al. (3) simulated the evolution of knotted vortices in the simply connected  
19 bulk of a superfluid using the Gross-Pitaevskii equation. Starting from randomly perturbed ideal shapes  
20 (4), Kleckner et al. have found that knots and links always untie into independent unknots by decreasing  
21 monotonically their number of crossings. As a typical example we show in Figure S1a the decay of the  $6_2$   
22 knot. It involves the rewiring of the crossings inside the dashed circles and leads through the Solomon link,  
23 the trefoil knot, and the Hopf link to the unknot which finally collapses.

24 **B. Experimental observations.** The final collapse of unknotted vortex loops was observed experimentally  
25 (1, 5). In these experiments, the superfluid vortices were initiated by a thermal counter-flow generated  
26 by a wire heater located at the bottom of the helium tank. The vortices were detected optically using  
27 very small hydrogen crystallites ( $1\mu\text{m}$  in size) illuminated with a thin sheet of a laser light. They were  
28 organized in chains because they were trapped in singular cores of the vortices (see S1b). The rewiring of  
29 the colliding segments of the entangled vortices was inferred from observation of abnormally fast movements  
30 of crystallites located in the vicinity of the collision point such as the green and orange ones in Figure  
31 S1b. Using this visualisation method, Bewley et al. (6) observed also independent superfluid vortex loops  
32 (unknots) resulting from the decay of knots and links and pointed out that they shrink and collapse thanks  
33 to the dissipation (see Figure S1c).

34 The conclusion of these theoretical and experimental works was that the knotted or linked entanglements  
35 of superfluid vortices decay into the defect-less ground state.

### 36 2. Topological decay of entanglements of disclinations in nematics

37 **A. Occurrence of disclinations in nematics.** The nematic mesophase owes its name to disclinations of  
38 rank  $m = 1/2$  (7) which appear in an optical microscope as *thin threads* or  $\nu\eta\mu\alpha$  in Greek (8) (see Figure  
39 S2). Disclinations are ubiquitous (9) in nematics because they can be generated, stretched and entangled  
40 easily by a mechanical stirring. Alternatively, disclination can also be generated in abundance during the  
41 symmetry breaking Isotropic-Nematic transition (10, 11).

42 **B. Genesis of entanglements generated by the Isotropic-Nematic phase transition.** In the case of the  
43 entanglement shown in Figures S2c-h the Isotropic-Nematic transition was driven by a thermal quench  
44 from the isotropic phase (see Movie S1). The geometry of the sample depicted in Figure S2a is the same as  
45 the one used in experiments with the 5CB/CB15 cholesteric mixtures. Due to the very small thickness  
46 of the mica sheets ( $\approx 50\mu\text{m}$ ) and of the nematic droplet ( $h_{\text{min}} \approx 100\mu\text{m}$ ) the rate of cooling due to the  
47 contact with ambient air is of the order of  $5\text{ deg } C/s$ .

48 Let us stress that in this experiment the azimuthal anchoring directions on the both mica sheets are the  
49 same: parallel to the x axis. In this geometry, in the ground state the director field is uniform :  $\mathbf{n}(z) = (1, 0, 0)$ .  
50 After the quench from the Isotropic phase, two other states compatible with the anchoring conditions are  
51 possible:  $\mathbf{n}(z) = (\cos(2\pi z/h), \sin(2\pi z/h), 0)$  (right-hand helix) and  $\mathbf{n}(z) = (\cos(2\pi z/h), -\sin(2\pi z/h), 0)$   
52 (left-hand helix). These excited states are separated from the ground state by  $m = 1/2$  disclinations  
53 depicted in Figures S2i and j.

54 **C. Decay of entanglements generated by the Isotropic-Nematic phase transition.** After their genesis, the  
55 initially dense and topologically complex entanglements of disclination loops undergo the topological decay  
56 during which colliding segments of knotted, linked or twisted disclination loops are rewired (12) (see Figures  
57 S2c-h). The rewiring of the colliding crossings in nematics is driven elastically i.e. it lowers the energy of  
58 disclinations proportional to their length.

59 In a simply connected nematic bulk, this topological decay driven by the tension of disclinations leads  
60 first to a collection of unlinked unknots (see Figure S2g) that subsequently shrink and collapse individually  
61 (see Movie S1). The topological decay ends when the defect-less ground state of the nematic is recovered  
62 (see Figure S2h).

63 Let us stress that the outcome of the decay process would be different if a polymer fiber was immersed  
64 in the nematic. If this is the case, the fiber alters the simply connected topology of the nematic so that in  
65 its presence, the topological decay of the dense entanglement of disclinations leads not to the defect-less  
66 ground state by to a necklace-like state made of disclination loops (unknots) tethered on the fiber (13).

### 67 3. Topological decay of entanglements of dislocations produced by the Isotropic-Cholesteric 68 phase transition

69 **A. Geometry of experiments.** The experimental setup used in the present study is depicted schematically  
70 in Figure S3c. It consists of two cylindrical mica sheets separated by a variable distance  $h_{min}$ . The sample,  
71 a droplet of a mixture of the nematic 5CB with the chiral compound CB15, is held by capillarity between  
72 them. Surfaces of the mica sheets orient the molecules of the liquid crystal in an *anchoring direction* parallel  
73 to them so that the axis of the cholesteric helix is parallel to the z axis. For the sake of simplicity we  
74 suppose that the anchoring direction is the same on both surfaces, for example parallel to the x axis (see  
75 Figure S3e).

76 **B. Two types of dislocations.** In this crossed cylinders geometry, the ground state shown in Figure S3d is  
77 made of annular fields indexed with the number  $N$  indicating the number of full cholesteric pitches located  
78 between the mica surfaces (14). The helical director field  $\mathbf{n}$  (unit vector parallel to the local orientation of  
79 molecules) inside the fields labeled  $N = 2$ ,  $N = 3$  and  $N = 4$  in Figure S3d is thus given by :

$$80 \quad \mathbf{n} = (\cos\varphi, \sin\varphi, 0) \quad [1]$$

81 with  $\varphi = N2\pi z/h(r)$  where  $h(r)$  is the local thickness of the cylinder/cylinder gap and  $N = 2, 3, 4$ .

82 **B.1. Non singular dislocations with the Burgers vector  $b=p$ .** For readers familiar with the solid state physics,  
83 the frontiers between the  $N$  and  $N-1$  fields in Figures S3d and e appear as analogous to crystal dislocations  
84 with the Burgers vector  $b$  equal to the full cholesteric pitch  $p$ .

85 If the director field  $\mathbf{n}$  was constrained to stay in the (x,y) plane, then the order parameter of the cholesteric  
86 could be represented by the complex function  $\Psi = e^{i\varphi(z)}$  like the order parameter of the superfluid state.  
87 Let us stress that in cholesterics, the phase  $\varphi$  has a physical meaning: it corresponds to the azimuthal angle  
88 defined in Figure S3f. In this approximation, the linear topological defects between the adjacent  $N-1$  and  
89  $N$  fields would be analogous to the superfluid vortices because on circuits surrounding them (for example  
90 ABCD in Figure S3e) the phase  $\varphi$  varies by  $2\pi$ . If this analogy with the superfluid vortices was fully true  
91 then the circular coaxial defect lines of the cholesteric visible in Figures 1 c and f of the Main Document  
92 would have singular cores like the superfluid vortices.

93 Since the pioneer works of Kleman and Friedel (15) and of Toulouse and Kleman (16) it is well known  
94 that this analogy is wrong : the core of dislocations with the Burgers vector  $b = p$ , known as *thick* or *double*,  
95 is non singular because the director field  $\mathbf{n}$  evolves not in two but in three dimensions as it depicted in  
96 Figure S3e. Its orientation is given by two angles : the azimuthal angle  $\varphi$  and the polar angle  $\theta$  defined in  
97 Figure S3f.

98 **B.2. Singular dislocations with the Burgers vector  $b = p/2$ .** On the contrary, dislocations with the Burgers  
99 vector  $b = p/2$  known as *thin* or *simple*, which are also possible in the geometry of Figure S3c, are analogous  
100 to the  $m = 1/2$  disclinations in nematics (see the section "Topological decay of entanglements of disclinations  
101 in nematics" above) so that they must have singular cores (15, 16). For this reason, knots and links made  
102 of them are unstable with respect to the rewiring of their crossings and their decay leads always to the  
103 defect-less ground state.

104 **C. The target-like ground state.** It can be shown (see ref.(14)) that in the ground state corresponding to  
 105 the minimum of the elastic distortion, the radii  $r_N$  of the circular concentric  $b = p$  dislocations are given by  
 106 :

$$107 \quad r_N^2 \approx 2R_m p \left( N - \frac{1}{2} - \frac{h_{min}}{p} \right) \quad [2]$$

108 where  $h_{min}$  is the minimal thickness of the gap,  $R_m$  is the radius of curvature of the cylindrical mica sheets  
 109 and  $N=1,2,3,\dots$  is the index of dislocation loops. The presence of the concentric dislocation loops in the  
 110 gap with the variable thickness  $h(r) = h_{min} + r^2/(2R)$  is thus a geometrical and topological necessity: they  
 111 separate fields with  $N-1$  and  $N$  full cholesteric pitches lodged in the gap between the cylindrical mica sheets  
 112 (14, 17).

113 **D. The trefoil knot of unusual shape and its decay to the Hopf link.** Let us note that in Figure 1c of the  
 114 Main Document, the circular dislocation loops are not independent but connected into *superloops* by radial  
 115 pairs of crossed dislocations such as the one in the insert of Figure 1c of the Main Document. It has been  
 116 shown previously (14, 18) that thanks to these crossings, the superloops are equivalent topologically to  
 117 knots or links having well defined unusual shapes. As an example we show in Figure S3b the trefoil knot. It  
 118 is composed of two circular loops, with radii  $r_3$  and  $r_4$  given by equation 2, interconnected by three radially  
 119 oriented crossed pairs of dislocations. Let us stress that this configuration is stable as long as the minimal  
 120 thickness  $h_{min}$  is smaller than  $5p/2$ , provided that the crossings are not rewired through interaction with  
 121 kinks (14) (see the SI Appendix Section "Absorption of minimal loop due to a lethal encounter with a  $+p/2$   
 122 kink" below) .

123 The rewiring of one of its three crossings transforms the trefoil knot into the Hopf link made of the same  
 124 two circular loops that stay interconnected by the two remaining crossings.

125 **E. The Hopf necklace.** When the minimal thickness  $h_{min}$  gets larger than  $5p/2$  (but remains smaller than  
 126  $7p/2$ ), the  $N=3$  loop is no more stable and the configuration of the Hopf link changes. The radius  $r_3$  of the  
 127  $N=3$  loop given by equation 2 is reduced to zero so that the two radial crossed pairs are joined into one  
 128 bow-like pair of dislocations crossed twice. Subsequently, the length of this bow-like pair is reduced for  
 129 energetical reasons and the Hopf link takes the very asymmetric shape labeled in Figure S3e as *the Hopf*  
 130 *necklace* which is made of the large circular  $N=4$  cargo loop with one minimal loop tethered on it.

131 The Hopf necklace in Figure S3e has the following features:

- 132 1. it exists only in the interval  $5p/2 < h_{min} < 7p/2$
- 133 2. its energy is larger than that of the target-like pattern
- 134 3. it is metastable because the minimal loop can be absorbed by the cargo loops as explained in the SI  
 135 Appendix Section "Absorption of minimal loop due to a lethal encounter with a  $+p/2$  kink"
- 136 4. it is absent in the unlinking pathway of the superfluid vortex knots depicted in Figure S3a (3, 19).

137 Let us stress that the first observation of the Hopf necklace was made by Bouligand (20) and its topology  
 138 was discusses shortly later by Bouligand et al. (21). Generation of the Hopf necklace by the decay of the  
 139 trefoil knot depicted in Figure S3b was reported recently (22).

140 At the end of the reference (22) we mentioned shortly that the topological decay of dense entanglements  
 141 of dislocations in the cylinder/cylinder confinement leads to a generalized version of the Hopf necklace in  
 142 which instead of just one, many minimal loops are tethered on the circular loops of the ground state. The  
 143 principal aim of the Main Document of this paper is to explore this phenomenon in more details and to  
 144 understand its origin.

145 **F. Genesis of necklaces in a thin sample with a small cholesteric pitch.** When the gap between the  
 146 cylindrical mica sheets is filled not with the pure nematic 5CB but with a cholesteric mixture 5CB/CB15,  
 147 the cooling from the isotropic phase produces a very complex entanglement of interconnected  $b = p/2$  and  
 148  $b = p$  dislocations (see Figures S4 c-f, S8 and Movies S2 and S3). The  $b=p/2$  dislocations, like the  $m = 1/2$   
 149 disclinations in nematics considered in section 2, have singular cores and appear as thin lines similar to the  
 150 nematic disclinations.

151 Remarkably, at the beginning of the decay (see Figures S4 e and f) the  $b = p$  dislocations are frequently  
 152 associated in pairs called Lehmann clusters with the total Burgers vector  $b = p - p = 0$ . These Lehmann  
 153 clusters are attached by one or two of their ends to the  $b = p/2$  dislocations (see Figure S4d).

154 During the subsequent decay, the size (length) of the Lehmann clusters is shrinking. Independent clusters  
 155 collapse but those which are linked with other cluster (pointed by small blue arrows in Figure S4f) reach  
 156 their minimal size. The tethered minimal loops are generated by this means. This mechanism leads to  
 157 generation of the necklace state with minimal loops pointed by blue arrows in Figure S4g.

158 **G. Genesis of necklaces in a thick sample with a large cholesteric pitch.** The second example of genera-  
 159 tion of necklaces by the isotropic - cholesteric transition is shown in Movie S3. The cholesteric pitch here is  
 160 very large ( $p_o = 40\mu m$ ) and the minimal thickness of the cylinder/cylinder gap is of the order of  $10p_o$ . The  
 161 three dimensional structure of necklaces can be resolved by observations with a short field depth objectives.

## 162 4. Geometry of necklaces

### 163 A. Three-dimensional structure of necklaces.

164 **A.1. Thin samples.** In Figure S5a, a necklace is seen from the  $z$  direction orthogonal to the  $(x,y)$  plane of the  
 165 cholesteric layer. Its three-dimensional structure, resolved using an objective with a short field depth, is  
 166 represented schematically by the perspective view in Figure S5b in which a circular cargo loop is charged  
 167 with five minimal loops tethered on its  $+p$  kinks. The label  $+p$  indicates that the  $z$  level of the cargo loop  
 168 rises by  $\Delta z = +p$  when the cargo loop is traveled in the clockwise direction indicated by the large arrow.

169 Let  $i$  be the index of the kinks and  $\Delta z_i$  the corresponding change of the  $z$  level. In the case of the  
 170 necklace state represented in Figure S5a one has :

$$171 \sum_{i=1}^{i=11} \Delta z_i = -p \quad [3]$$

172 This non zero result is the fingerprint of the helical symmetry of the cholesteric phase (17, 21, 23).

173 **A.2. Thick samples.** In thick samples ( $h_{min} \approx 10p_o$ ) the minimal loops are not always scattered along the  
 174 cargo loops but form also small chain-like sets similar to the one in Figure S6a. This view in a microscope  
 175 shows four minimal loops tethered on the oblique segment OA of the cargo loop defined in Figure S6b. The  
 176 three-dimensional structure of the necklace unveiled in this perspective view is inferred from the deformation  
 177 of the necklace (see Figures S6a, d and e) by the shear flow driven by the displacement  $\Delta y$  of the upper  
 178 mica sheet in the  $y$  direction (see also Movie S7). The genesis of such chain-like sets of minimal loops is  
 179 explained in Figures 5h, i and j of the Main Document where the link [8] with numerator closure is split  
 180 into four Hopf links [2].

181 **B. Diameter of the minimal loops.** *The minimal loops tethered on kinks of cargo loops do not collapse*  
 182 *because they are submitted to a repulsive interaction with kinks.* To understand the origin of this repulsive  
 183 force let us approximate the kink by the double twist cylinder (see ref.(24)) of radius  $r_{dt}$  depicted in Figure  
 184 S7 (see Movie S8). In the vicinity of the  $z$  axis, the director field is expressed in cylindrical coordinates as:

$$185 \mathbf{n}(r, \varphi, z) = [0, \cos \theta(r), \sin \theta(r)] \quad [4]$$

186 where  $\theta(r)$  is the angle between the director  $\mathbf{n}$  and the z axis varying from  $\theta(0) = 0$  to  $\theta(r_{dte}) = \pi/2$  (see  
187 Figure S7).

188 Let us suppose in a first approximation that

$$189 \quad \theta(r) = qr \quad [5]$$

190 with

$$191 \quad q = \frac{2\pi}{p} = \frac{2\pi}{4r_{dte}} \quad [6]$$

192 With the density of the distortion energy per unit volume given by (24)

$$193 \quad f = \frac{K_2}{2} \left( q_o - \frac{\partial\theta}{\partial r} - \frac{1}{r} \sin\theta \cos\theta \right) + \frac{K_3}{2} \frac{\sin^4\theta}{r^2} - \frac{K_{24}}{r} \frac{\partial \sin^2\theta}{\partial r} \quad [7]$$

194 one can calculate the energy of the double twist cylinder of height  $p_o$  as the integral:

$$195 \quad F_{dte} = p_o \int_0^{r_{dte}} f 2\pi r dr = p_o \frac{\pi K_2}{8} \left[ C - (8 + 2\pi^2)\rho + \pi^2\rho^2 \right] \quad [8]$$

196 where C is a numerical constant depending on the ratio  $K_{24}/K_2$  and  $\rho = q_o/q = r_{dte}/(p_o/4)$  is proportional  
197 to the radius of the double twist cylinder defined by equations 5 and 6.

198  $F_{dte}(\rho)$  has a minimum for  $\rho = 1 + 4/\pi^2 \approx 1.4$  i.e. for  $r_{dte} \approx 0.35p_o$ . This means that the radius of the  
199 double-twist cylinder is smaller than  $p_o/4$ .

200 The total energy of the system kink+minimal loop can be written as

$$201 \quad F_{kink+ml} = F_{dte}(r_{dte}) + 2\pi r_{ml} T \quad [9]$$

202 Assuming that the radius  $r_{ml}$  of the minimal loop can be approximated as  $r_{ml} \approx r_{dte} + p_o/4$  one can  
203 calculate that the minimum of the total energy  $F_{kink+ml}$  occurs for

$$204 \quad r_{ml} = \frac{p_o}{4} \frac{4 + 2\pi^2 - 8\tilde{T}}{\pi^2} \quad [10]$$

205 where  $\tilde{T} = T/K_2$ . Knowing from experiments that  $r_{ml} \approx p_o/2$  we can infer that  $T \approx K_2/2$ .

## 206 C. Number of minimal loops and its evolution.

207 **C.1. Number of minimal loops at the end of the decay.** The number  $M_\infty$  of the minimal loops tethered on the  
208 coaxial circular cargo loops at the end of the decay can be estimated as follows. In Figure 2g of the Main  
209 Document, the distance between the minimal loops tethered on dislocations separating N-1 and N fields  
210 is of the order of  $\Delta r = r_N - r_{N-1}$  (see for example the circular dislocation separating the N=5 and N=6  
211 fields). Therefore, the total number M of the minimal loops inside the circle of radius  $r_{10}$  is given by

$$212 \quad M_\infty \approx \sum_{N=3}^{N=10} \frac{2\pi r_N}{r_N - r_{N-1}} \quad [11]$$

213 Using equation 2 with  $h_{min}/p = 1$ , one obtains  $M \approx 475$  which agrees in order of magnitude with  
214 observations.

215 **C.2. Evolution of the density of minimal loops.** The series of six pictures in Figure S8a shows that the number  
216  $M(t)$  of minimal loops evolves during the decay. Initially it grows from zero when the minimal loops are  
217 generated by the mechanisms discussed in section "How the minimal loops are formed ?" of the Main  
218 Document. Later, it passes through a maximum  $M_{max}$  and, finally, in the limit  $t \rightarrow \infty$  it decreases to its  
219 equilibrium value  $M_\infty$ . The final decrease of  $M(t)$  is due to the process of absorption of the minimal loops  
220 by the cargo loop described below.

221 **C.3. Absorption of a minimal loop by the cargo loop due to a lethal encounter with a  $+p/2$  kink.** The absorption  
222 of minimal loops by the cargo loop is due to their encounters with  $-p/2$  kinks depicted in Figure S9.  
223 Necklaces, threaten by such encounters, are therefore metastable. Nevertheless they can be persistent  
224 because the kinks not very mobile.

225 **C.4. Collapse of a cargo loop with minimal loops tethered on it.** The encounters between the minimal loops  
226 and the kinks are favored by shrinking of the cargo loops. In the example shown in Figure S10, the cargo  
227 loop belongs to the target-like pattern of coaxial dislocation loops inside the cylinder/cylinder gap. Under a  
228 small increase of the minimal thickness  $h_{min}$ , its equilibrium radius  $r_N$  can be reduced to zero (see equation  
229 (2) of the Main Document) so that this cargo loops shrinks progressively and distances between the minimal  
230 loops and kinks are reduced too.

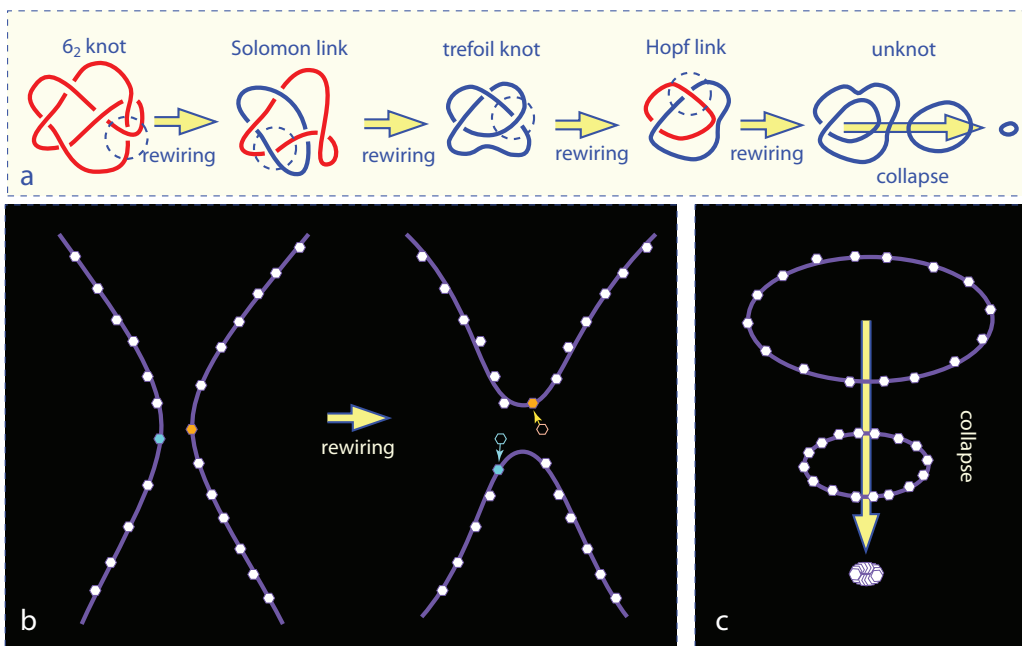


**Fig. S1.** Decay of knots made of superfluid vortices. a) Theoretical decay of the  $6_2$  knot leads through the Solomon link, trefoil knot and Hopf link to the unknot that finally shrinks and collapses (3, 19). b) Optical observation of hydrogen microcrystallites trapped in cores of the superfluid vortices allows to detect the rewiring processes. Here, the orange and blue crystallites move rapidly during the rewiring (6). c) Collapse of an unknotted vortex loop visualized by means of the trapped hydrogen crystallites.

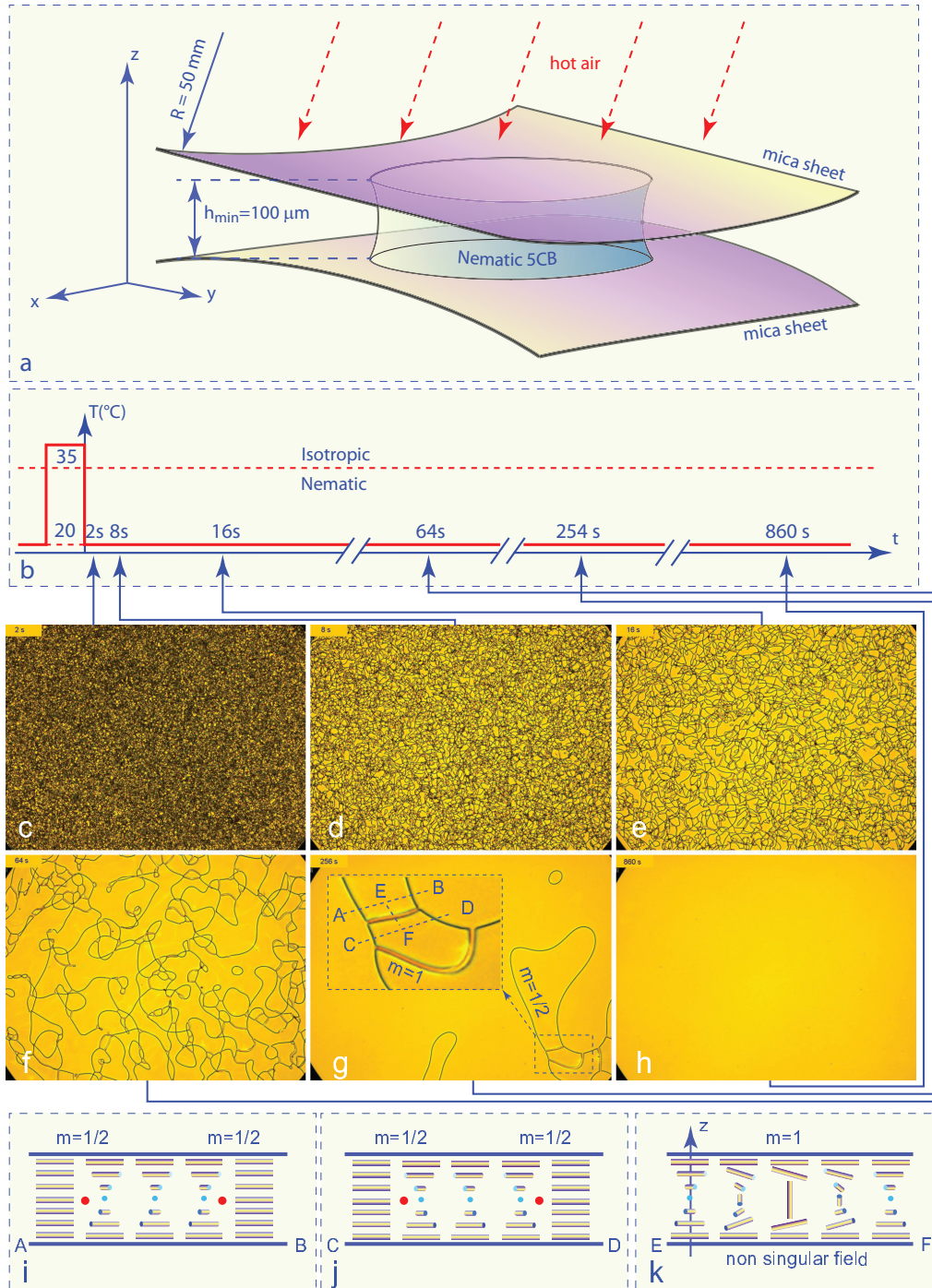


**Fig. S2.** Decay of an entanglement of  $m = 1/2$  disclinations generated in the gap between the mica sheets by the Isotropic-Nematic phase transition. a) Geometry of the experiment: droplet of 5CB confined by capillarity between cylindrical mica sheet. The sample is heated by a stream of hot air until the Nematic-Isotropic transition occurs. The subsequent quench to the Nematic phase is due to the spontaneous cooling at ambient temperature. b) Variation of temperature in time. c-g) Entanglement at  $t = 2, 8, 16, 64$  and  $256$  s after its genesis. h) At  $t = 860$  s, the defect-less ground state is recovered. i) Cross section of the texture along the AB line defined in (g). The red circles indicate singularities of the  $m = 1/2$  disclination. j) Cross section of the texture along the CD line defined in (g). The red circles indicate singularities of the  $m = 1/2$  disclination. h) Cross section of the  $m = 1$  disclination along the EF line defined in (g). The director field  $\mathbf{n}(\mathbf{r})$  is non singular here thanks to the escape in the third dimension  $z$ .

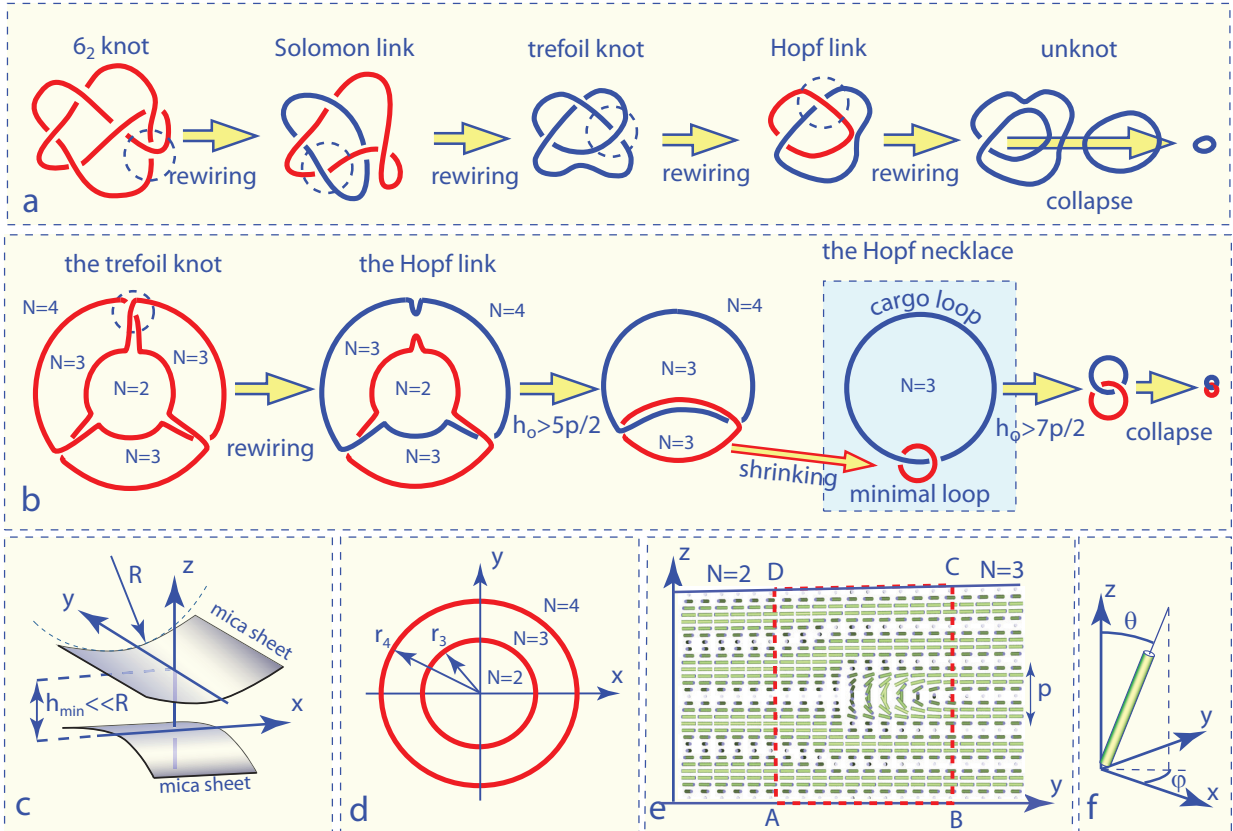


**Fig. S3.** Decay of individual knots and links made of linear topological defects. a) Superfluid vortices: the decay of the  $6_2$  knot leads through the Solomon link, trefoil knot and Hopf link to the unknot that finally shrinks and collapses (3, 6, 19). b) Dislocations in cholesterics: decay of the trefoil knot made of two circular dislocations interconnected by three crossings. Rewiring of one crossings leads to the Hopf link. The detailed shape of the Hopf link varies with the minimal thickness  $h_{min}$  of the gap. In the interval  $5p/2 < h_{min} < 7p/2$  the Hopf link takes the necklace-like shape made of the minimal loop tethered on the cargo loop. This Hopf necklace is the metastable remnant of the decay of the trefoil knot. For  $7p/2 < h_{min}$ , the Hopf necklace collapses. c) Geometry of experiments with dislocations in a cholesteric layer confined between cylindrical crossed mica sheets (14). d) In equilibrium, dislocation loops have shapes of concentric circles with radii  $r_N$  given by equation 2. e) Cross section of the cholesteric layer: fields with  $N=2$  and  $N=3$  full cholesteric pitches are separated by a dislocation with the Burgers vector  $b = p$ . The core of this dislocation is non singular thanks to the escape of the twisted director field into the third dimension  $z$ . f) Definition of the polar  $\theta$  and azimuthal  $\varphi$  angles.

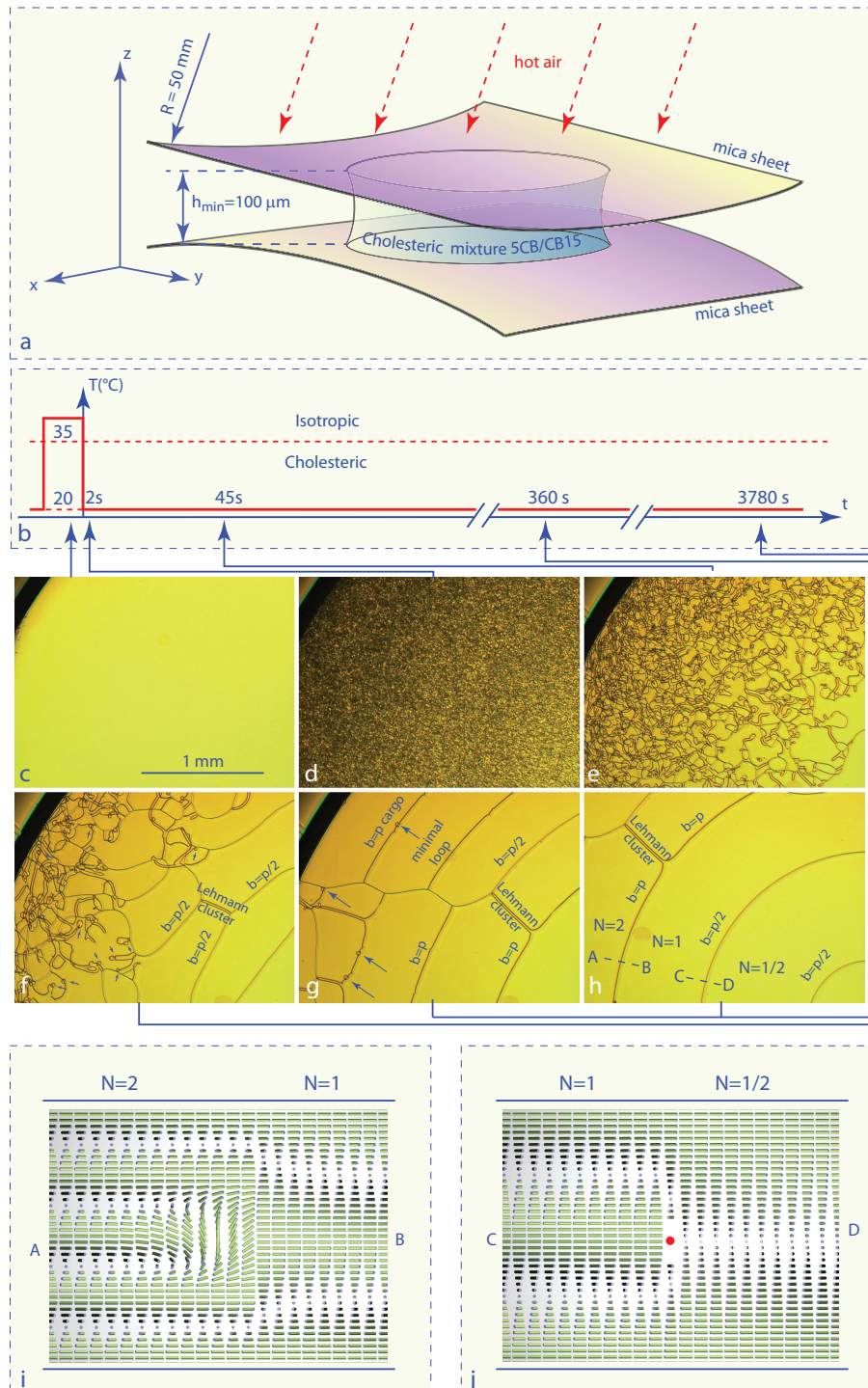


**Fig. S4.** Generation of the necklace state through the Isotropic-Cholesteric phase transition. a) Geometry of the experiment: droplet of a 5CB/CB15 cholesteric mixture confined by capillarity between cylindrical mica sheet. The sample is heated by a stream of hot air until the Cholesteric-Isotropic transition occurs. The subsequent quench to the Cholesteric phase is due to the spontaneous cooling at ambient temperature. b) Variation of the temperature with time. c) Isotropic phase of the 5CB/CB15 mixture. d) Dense entanglement of dislocations produced by the Isotropic-Cholesteric phase transition. d-g) Decay of the entanglement made of the single ( $b=p/2$ ) and double ( $b=p$ ) dislocations. f) Few minimal loops tethered on the  $b=p$  dislocations are indicated by arrows. g) Final state of the decay in the thick part of the cylinder/cylinder gap. The necklace state involves only the  $b=p$  dislocations. h) Final state of the decay in the thinnest part of the cylinder/cylinder gap. The  $b=p/2$  dislocations present here do not form tethered loops. i) Cross section of the dislocation  $b = p$  along the line AB defined in (h). j) Cross section of the dislocation  $b = p/2$  along the line CD defined in (h).

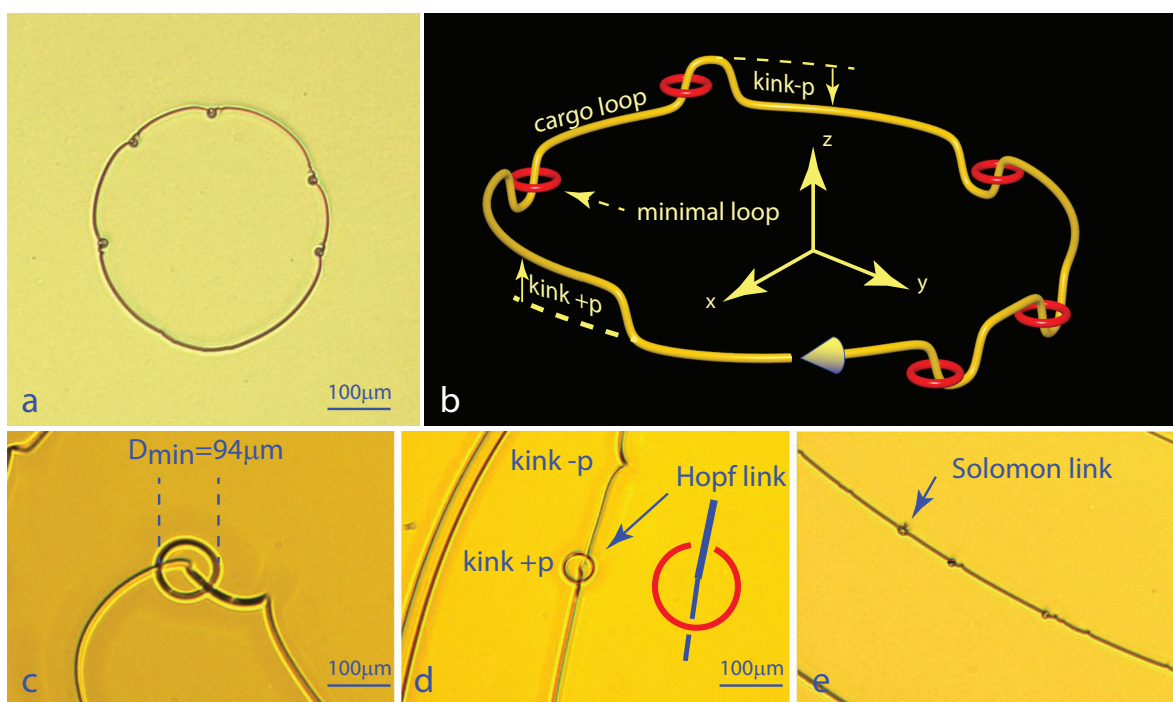


**Fig. S5.** Geometry of the necklace state in a thin sample. a) View in a microscope of a necklace made of a circular cargo loop charged with five minimal loops. b) Perspective view of the necklace. The minimal loops are tethered on  $+p$  kinks which in a first approximation can be seen as vertical screw dislocations of length  $p$ . c-e) The diameter of the minimal loops is of the order of the cholesteric pitch  $p$ :  $D_{min} \approx p$ . It varies with the concentration  $c_{15CB}$  of the chiral compound CB15 in the nematic 5CB: (c)  $c_{15CB} = 0.4\%$ , (d)  $c_{15CB} = 0.86\%$  (e)  $c_{15CB} = 3.4\%$ . d) Occurrence (very scarce) of the Solomon configuration of the necklace state.

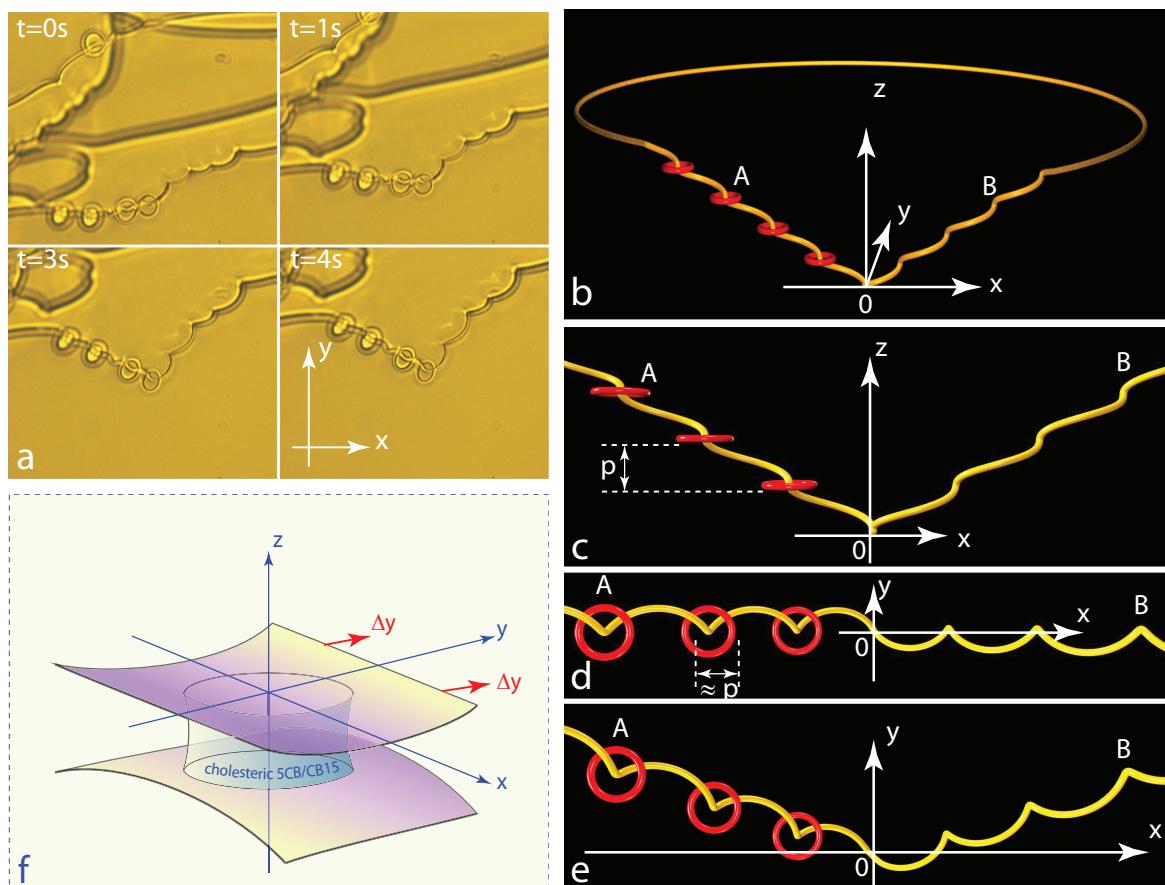


**Fig. S6.** Three-dimensional structure of a necklace generated in a thick sample. a) View in a microscope of the necklace submitted to a shear flow due to the displacement  $\Delta y$  of the upper mica sheet (defined in (f)). Deformation of the necklace unveils its three-dimensional structure represented in (b), (c) and (d). b) Perspective view of a model of the necklace. c) View of the model from the y direction. The minimal loops of diameter  $\approx p$  are tethered on vertical segments of the cargo loop. d) View of the model from the z direction. e) The same after the deformation of the necklace due to the shear flow.

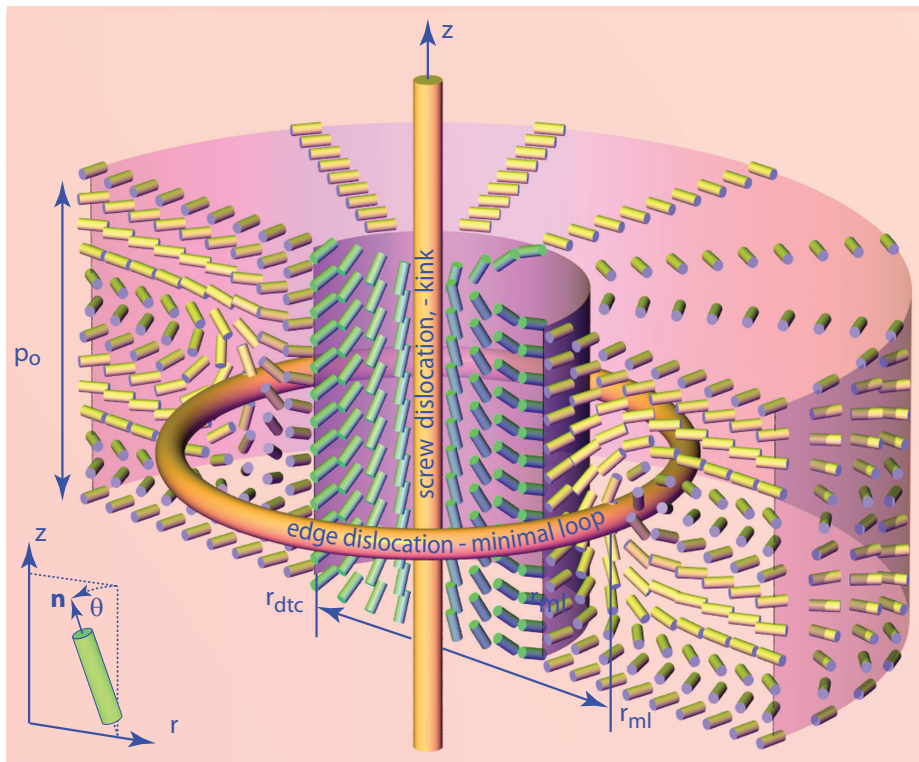


**Fig. S7.** Minimal loop of radius  $r_{ml}$  tethered on the kink of the cargo loop. The kink is a quasi vertical segment of the cargo loop and can be approximated as a vertical screw dislocation with the Burgers vector  $b = p$ . Thanks to its action, the director field  $\mathbf{n}$  acquires the symmetry of revolution around the  $z$  axis : in cylindrical coordinates  $(r, \psi, z)$  it is independent of the azimuthal angle  $\psi$ :  $\mathbf{n} = \mathbf{n}(r, z)$ . Moreover, in the vicinity of the  $z$  axis inside the double twist cylinder of radius  $r_{dtc}$  for  $0 < r < r_{dtc}$ , it can be approximated by the double twist texture independent of  $z$ :  $\mathbf{n} = (0, \sin(qr), \cos(qr))$  with  $q = (\pi/2)/r_{dtc}$ .

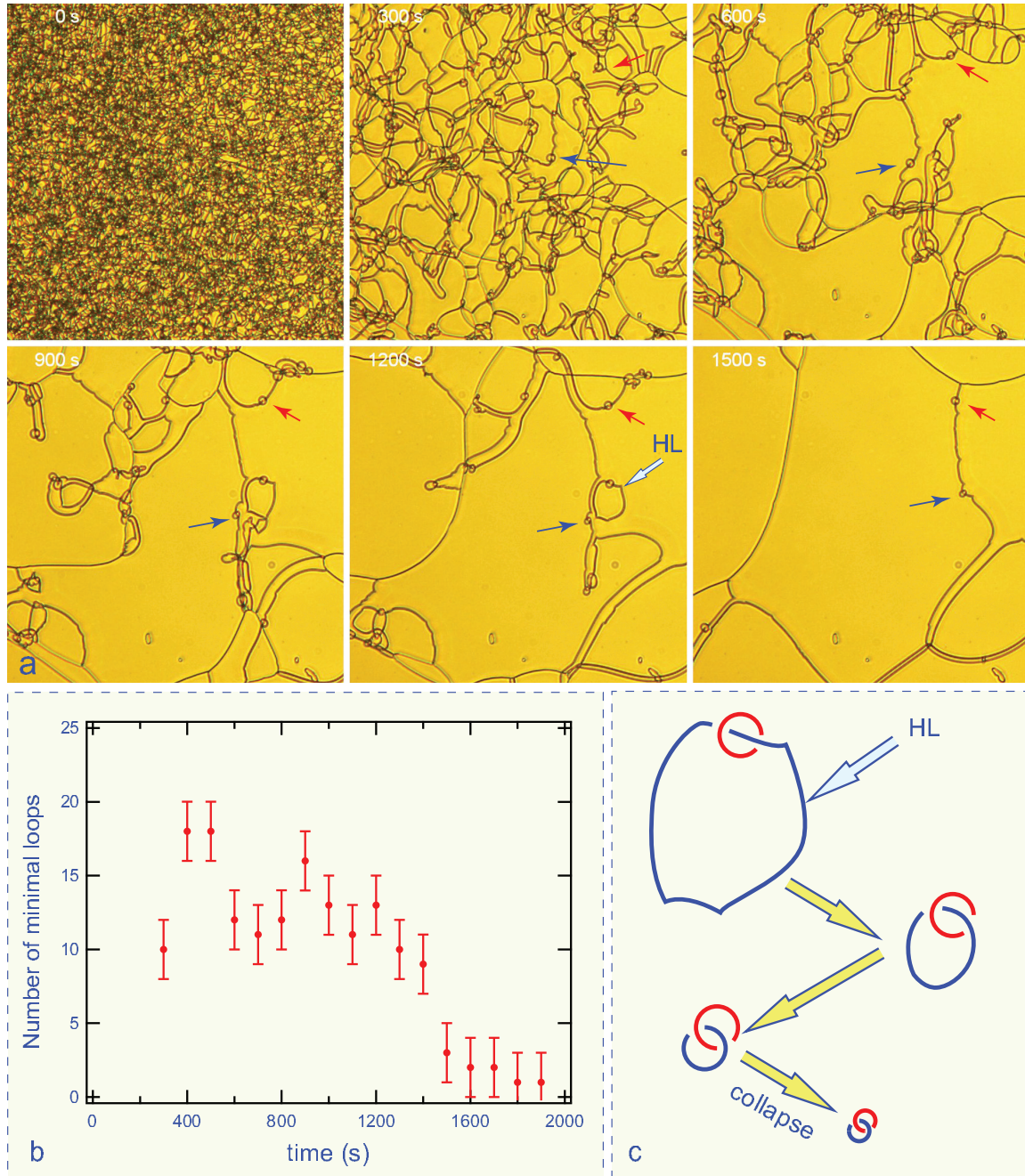


**Fig. S8.** Evolution of the number  $M(t)$  of minimal loops after during the decay of an entanglement generated during the thermal quench from the isotropic to the cholesteric phase. a) Evolution of the dislocations' pattern made of  $b = p$  and  $b = p/2$  dislocations. Minimal loops marked with the red blue arrows are conserved from  $t = 300$ s to  $t = 1500$ s. All other minimal minimal loops have an ephemeral existence. For example, the one marked with the large arrow belongs to the Hopf link of small size labeled HL which shrinks and collapses as shown in (c). b) Plot  $M(t)$ . c) Evolution of the shape and size of the Hopf link HL marked with the large blue arrow in the picture "1200s" in (a).

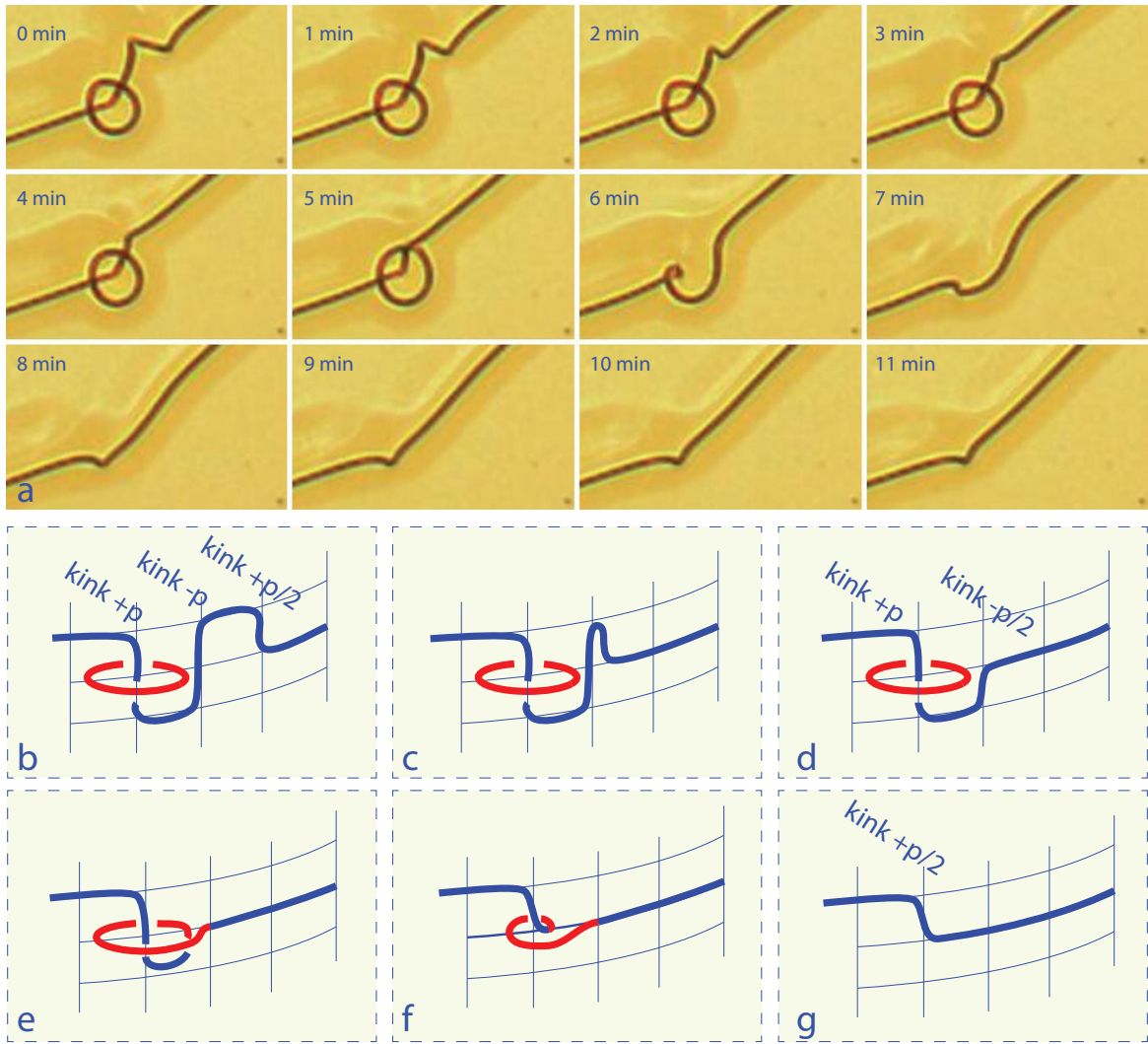


**Fig. S9.** Lethal encounter between a minimal loop and a  $-p/2$  kink resulting in absorption of the minimal loop by the cargo loop. a) View in a microscope, b-g) Perspective view.

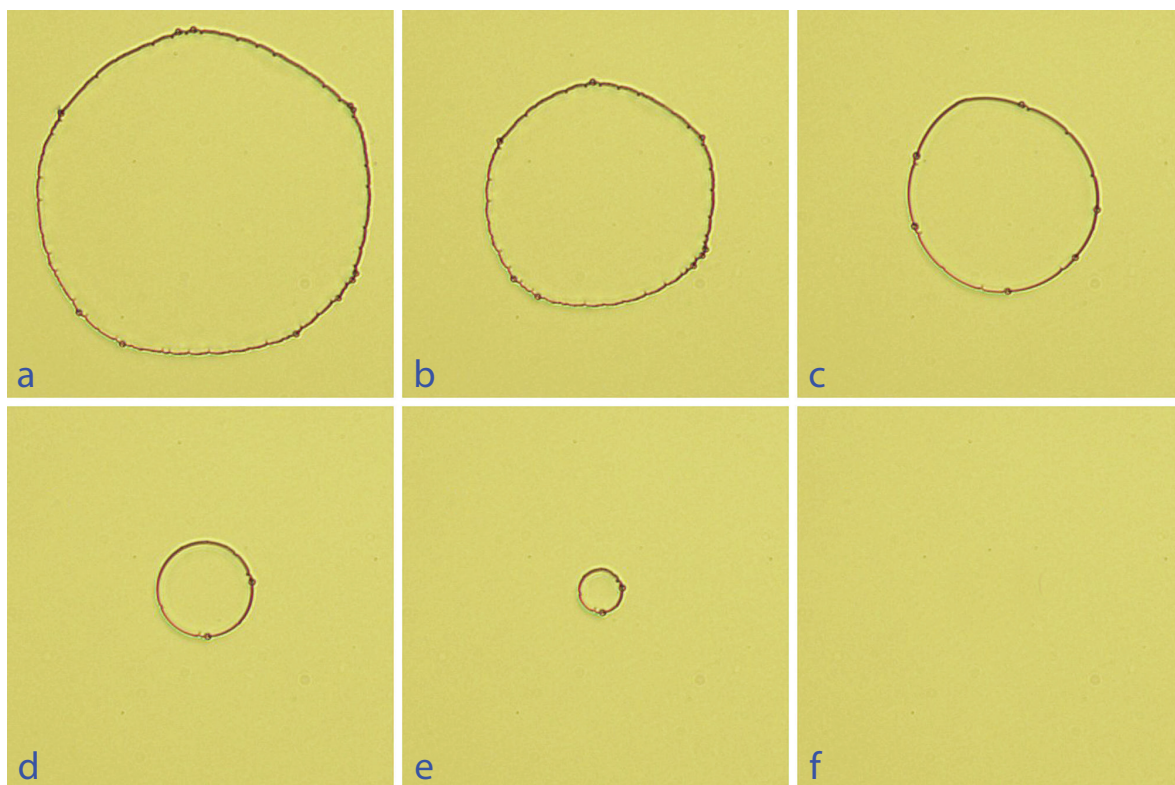


**Fig. S10.** Collapse of a necklace. a) The necklace made of 11 minimal loops tethered on the central loop from the target-like pattern. b-e) Decrease of the number of minimal loops due to lethal encounters with links (see Figure S9). These encounters are favored by the shrinking of the cargo loop under a small increase of the minimal gap thickness  $h_{min}$ . e-f) Final collapse of the cargo loop.

231 **Movie S1.** Decay of an entanglement of disclinations generated during isotropic  $\rightarrow$  nematic  
232 transition leads to the defect-less ground state.

233 **Movie S2.** Decay of an entanglement of disclinations generated by the isotropic - cholesteric  
234 transition.

235 **Movie S3.** Decay of an entanglement of disclinations generated by the isotropic - cholesteric  
236 transition in a thick sample with a large pitch  $p = 40\mu m$ .

237 **Movie S4.** Decay of an entanglement of disclinations generated by a dilation-compression  
238 strain pulse leads to the necklace-like state made of minimal loops tethered on large cargo  
239 loops.

240 **Movie S5.** Second example of the necklace-like state generated by a dilation-compression  
241 strain pulse.

242 **Movie S6.** Necklace-like multicomponent link in a sample with a large pitch.

243 **Movie S7.** Deformation of a necklace by shear flow

244 **Movie S8.** Twisted structure of the director field in vicinity of the minimal edge dislocation  
245 loop tethered on the screw dislocation corresponding to the kink of the cargo loop.

246 **Movie S9.** Rewiring of the two component link [4] (Solomon link) into pair of the two [2]  
247 (Hopf) links.

248 **Movie S10.** Rewiring of the two component link [6] into pair of the two component [4] and  
249 [2] links.

250 **Movie S11.** Rewiring of the two component link [4] (Solomon link) into pair of the two [2]  
251 (Hopf) links.

252 **Movie S12.** Rewiring of the two component link [8] (double helix tangle with numerator  
253 closure) into four [2] links.

## 254 **References**

- 255 1. MS Paoletti, ME Fisher, KR Sreenivasan, DP Lathrop, Velocity statistics distinguish quantum  
256 turbulence from classical turbulence. *Phys. Rev. Lett.* **101**, 154501 (2008).
- 257 2. RP Feynman, Chapter ii application of quantum mechanics to liquid helium in *Progress in low*  
258 *temperature physics*. (Elsevier) Vol. 1, pp. 17–53 (1955).
- 259 3. D Kleckner, LH Kauffman, WT Irvine, How superfluid vortex knots untie. *Nat. Phys.* **12**, 650–655  
260 (2016).
- 261 4. P Pierański, In search of ideal knots. *Ideal knots* **19** (1998).
- 262 5. GP Bewley, DP Lathrop, KR Sreenivasan, Visualization of quantized vortices. *Nature* **441**, 588–588  
263 (2006).
- 264 6. GP Bewley, KR Sreenivasan, The decay of a quantized vortex ring and the influence of tracer particles.  
265 *J. Low Temp. Phys.* **156**, 84–94 (2009).
- 266 7. FC Frank, I. liquid crystals. on the theory of liquid crystals. *Discuss. Faraday Soc.* **25**, 19–28 (1958).
- 267 8. G Friedel, Les états mésomorphes de la matière. *Annales de physique* **9**, 273–474 (1922).

- 268 9. P Oswald, P Pieranski, *Nematic and cholesteric liquid crystals: concepts and physical properties*  
269 *illustrated by experiments*. (CRC press), (2005).
- 270 10. I Chuang, R Durrer, N Turok, B Yurke, Cosmology in the laboratory: Defect dynamics in liquid  
271 crystals. *Science* **251**, 1336–1342 (1991).
- 272 11. I Chuang, B Yurke, AN Pargellis, N Turok, Coarsening dynamics in uniaxial nematic liquid crystals.  
273 *Phys. Rev. E* **47**, 3343 (1993).
- 274 12. P Pieranski, MH Godinho, Collisions of monopoles, disclinations and dislocations. *The Eur. Phys. J.*  
275 *Special Top.* pp. 1–21 (2024).
- 276 13. M Dazza, L Cabeca, S Copar, MH Godinho, P Pieranski, Action of fields on captive disclination loops.  
277 *EPJE* **40**, 28 (2017).
- 278 14. P Pieranski, M Godinho, Unknots, knots, links and necklaces made of dislocations in cholesterics. *Liq.*  
279 *Cryst.* pp. 1–32 (2024).
- 280 15. M Kleman, J Friedel, Lignes de dislocations dans les cholestériques. *J. de Phys.* **30**, C4–43–C4–53  
281 (1969).
- 282 16. G Toulouse, M Kleman, Principles of a classification of defects in ordered media. *J. de Physique Lettres*  
283 **37**, L–149 (1976).
- 284 17. P Pieranski, Cholesteric dislocations in mica wedges. *Liq. Cryst. Rev.* **9**, 65–92 (2022).
- 285 18. P Pieranski, MH Godinho, Fertile metastability. *Liq. Cryst.* **50**, 1177–1192 (2023).
- 286 19. X Liu, RL Ricca, XF Li, Minimal unlinking pathways as geodesics in knot polynomial space. *Commun.*  
287 *Phys.* **3**, 136 (2020).
- 288 20. Y Bouligand, Recherches sur les textures des états mésomorphes. 6- dislocations coin et signification  
289 des cloisons de grandjean-cano dans les cholestériques. *J. de Physique* **35**, 959–981 (1974).
- 290 21. Y Bouligand, B Derrida, V Poénaru, Y Pomeau, G Toulouse, Distorsions with double topological  
291 character: the case of cholesterics. *J. de Physique* **39**, 863–867 (1978).
- 292 22. P Pieranski, MH Godinho, The toulouse-kleman homotopic classification of topological defects in  
293 ordered systems illustrated by experiments. *Comptes Rendus Physique* (2024).
- 294 23. I Smalyukh, O Lavrentovich, Three-dimensional director structures of defects in grandjean-cano wedges  
295 of cholesteric liquid crystals studied by fluorescence confocal polarizing microscopy. *Phys. Rev. E* **6**,  
296 051703 (2002).
- 297 24. M Kleman, O Lavrentovich, *Soft matter physics: an introduction*. (Springer, New york), 1 edition,  
298 (2001).